Thermalized dark radiation in the presence of a PBH: ΔN_{eff} and gravitational waves complementarity

Nayan Das,* Suruj Jyoti Das,† and Debasish Borah‡

Department of Physics, Indian Institute of Technology Guwahati, Assam 781039, India

(Received 15 July 2023; accepted 7 November 2023; published 30 November 2023)

We study the possibility of detecting dark radiation (DR) produced by a combination of interactions with the thermal bath and ultralight primordial black hole (PBH) evaporation in the early Universe. We show that the detection prospects via cosmic microwave background (CMB) measurements of the effective relativistic degrees of freedom ΔN_{eff} get enhanced in some part of the parameter space compared to the purely nonthermal case where DR is produced solely from a PBH. On the other hand, for a certain part of the parameter space, DR that initially decouples from the bath, followed by its production from PBH evaporation, can reenter the thermal bath leading to much tighter constraints on the PBH parameter space. We also discuss the complementary detection prospects via observation of stochastic gravitational waves (GW) sourced by PBH density perturbations. The complementary probes offered by CMB and GW observations keep the detection prospects of such light degrees of freedom very promising in spite of limited discovery prospects at particle physics experiments.

DOI: 10.1103/PhysRevD.108.095052

I. INTRODUCTION

The matter content in the present Universe is dominated by dark matter (DM) as suggested by numerous astrophysics- and cosmology-based observations [1,2]. While a fundamental particle with the required characteristics can give rise to DM, the dark sector, in general, can be much richer. For example, the dark sector can contain different light degrees of freedom, commonly referred to as dark radiation (DR) [3]. While their contribution to the overall energy budget of the present Universe is negligible, they can have different phenomenological significance as well as detection prospects. For example, a very light scalar or gauge boson can give rise to sizable self-interaction of DM, having the potential to solve the small-scale structure issues of the cold dark matter paradigm [4–6]. Other relativistic degrees of freedom may arise in different particle physics scenarios in the form of (pseudo) Goldstone boson, moduli fields, gravitons, light sterile neutrinos, Dirac active neutrinos, and so on.

Similar to radiation energy density at the present epoch, these light relativistic degrees of freedom typically contribute negligibly to the total energy budget. In spite of that, cosmological observations can tightly constrain their abundance. The presence of dark radiation can be probed at cosmic microwave background (CMB) experiments. Existing data from CMB experiments like Planck constrain such additional light species by putting limits on the effective degrees of freedom for neutrinos during the era of recombination ($z \sim 1100$) as [2]

$$N_{eff} = 2.99^{+0.34}_{-0.33} \tag{1}$$

at 2σ or 95% C.L. including baryon acoustic oscillation data. At 1σ C.L. it becomes more stringent for $N_{eff} = 2.99 \pm 0.17$. A similar bound also exists from big bang nucleosynthesis (BBN) $2.3 < N_{eff} < 3.4$ at 95% C.L. [7]. All these bounds are consistent with standard model (SM) predictions $N_{eff}^{SM} = 3.044$ [8–10]. (Note that Refs. [11–14] report a slightly higher value of N_{eff}^{SM} as 3.045.)[1] Future CMB experiment CMB stage IV (CMB-S4) is expected reach a much better sensitivity of $\Delta N_{eff} = N_{eff} - N_{eff}^{SM} = 0.06$ [16], taking it closer to the SM prediction. Similar precision measurements are also expected from other planned future experiments like SPT-3G [17] and Simons Observatory [18], as well as CMB-HD [19].

If dark radiation has sizable interactions with the SM bath, it can be thermalized in the early Universe, followed

*nayan.das@iitg.ac.in
†suruj@iitg.ac.in
‡dborah@iitg.ac.in

[1]A very recent paper [15] reports $N_{eff}^{SM} = 3.043$ by taking into account the next-to-leading order correction to $e^+e^- \leftrightarrow \nu_L\bar{\nu}_L$ interactions along with finite temperature QED corrections to the electromagnetic plasma density and effect of neutrino oscillations.

by decoupling at some stage. Depending upon the decoupling temperature and internal degrees of freedom, such dark radiation can have very specific predictions for $\Delta N_{\rm eff}$, which can either be ruled out by existing Planck data or can be probed at future experiments. On the other hand, if DR has feeble interactions with the SM bath, it will not be thermalized but can still be produced via freeze-in. The contribution to $\Delta N_{\rm eff}$ in such a case depends upon the DR-SM coupling. Even in the absence of any direct coupling between SM and DR, it is still possible for the latter to be produced in the early Universe purely due to gravitational effects. One such possibility arises when the early Universe has a sizable abundance of primordial black holes (PBHs). Depending upon the initial abundance of PBHs, such DR produced solely from PBH evaporation can contribute substantially to $\Delta N_{\rm eff}$ [20,21]. Similar works related to production of such light beyond the standard model (BSM) particles, including dark radiation from PBH evaporation and phenomenological implications, can be found in [22–28] and references therein. In the presence of DR, entire the PBH mass window in the ultralight ballpark, namely, $\sim 0.1 - 10^8$ g can be probed in future CMB experiments, while current Planck data rule out certain PBH masses with large initial fractions.

Motivated by this, in the present work we consider a hybrid scenario where dark radiation can be produced both from the thermal bath as well as from PBH evaporation. While a PBH can give an extra contribution to $\Delta N_{\rm eff}$, it can also dilute any initial $\Delta N_{\rm eff}$ generated thermally. Additionally, depending upon DR-SM interactions, PBH evaporation can lead to rethermalization of DR as well, putting new constraints on PBH parameters not obtained in earlier works carried out in the absence of additional DR-SM interactions. We first show the results by considering different types of dark radiation with specific decoupling temperatures and corresponding $\Delta N_{\rm eff}$. To illustrate the issue of rethermalization we consider the DR to be in the form of light Dirac neutrinos (right chiral part), although the generic conclusions reached here are valid for other types of DR as well which have sizable interactions with the SM bath. Assuming PBHs to dominate the Universe at early epochs such that the constraints from $\Delta N_{\rm eff}$ are the strongest, we also show the prospects of gravitational waves (GWs) complementarity in present and future experiments. The ultralight PBH considered in our work can lead to GW production due to PBH density fluctuations, keeping it in the observable ballpark of millihertz–kilohertz frequencies with peak amplitudes lying within reach of even LIGO-VIRGO, as well as several planned experiments. We find interesting complementarity between $\Delta N_{\rm eff}$ observations at CMB experiments and GW observations at present and near-future GW detectors.

This paper is organized as follows. In Sec. II, we briefly summarize the production of dark radiation from evaporating PBHs. In Sec. III, we consider DR production both from thermal bath and PBH evaporation with different examples of dark radiation. In Sec. IV, we consider Dirac active neutrinos as a specific example with effective four-fermion-type interactions with the SM bath and show the possibility of rethermalization and its implications. We discuss the gravitational waves complementarity in Sec. V and finally conclude in Sec. VI.

II. DARK RADIATION FROM A PBH

Considering PBHs to be formed in the early radiation-dominated Universe at a temperature, say $T_{\rm in}$, the initial mass of a PBH is related to the mass enclosed in the particle horizon and is given by [29–31]

$$m_{\rm in} = \frac{4\pi}{3}\gamma\frac{\rho_{\rm R}(T_{\rm in})}{H^3(T_{\rm in})}, \tag{2}$$

where $\gamma \approx 0.2$ [30], $\rho_{\rm R}(T_{\rm in})$ is the initial radiation density, and H is the Hubble expansion rate. The temperature of a black hole can be related to its mass as [32]

$$T_{\rm BH} = \frac{1}{8\pi G M_{\rm BH}} \approx 1.06\left(\frac{10^{13}\ \rm g}{M_{\rm BH}}\right)\ \rm GeV. \tag{3}$$

PBHs may dominate the energy density of the Universe depending on their initial abundance, characterized by the dimensionless parameter

$$\beta = \frac{\rho_{\rm BH}(T_{\rm in})}{\rho_{\rm R}(T_{\rm in})}. \tag{4}$$

Once PBHs form,[2] they lose mass through Hawking evaporation at a rate given by [38]

$$\frac{dM_{\rm BH}}{da} = -\frac{\epsilon(M_{\rm BH})\kappa}{aH}\left(\frac{1\ \rm g}{M_{\rm BH}}\right)^2. \tag{5}$$

Here a is the scale factor and $\kappa = 5.34 \times 10^{25}\ \rm g\,s^{-1}$ [21]. Because of only gravitational effects, production of all particles takes place, regardless of their interaction with other particles. The evaporation function $\epsilon(M_{\rm BH})$ [21] contains contributions from both SM and BSM particles. The temperature of the thermal plasma when the PBHs have completely disappeared can be found by integrating Eq. (5) and can be written as [39]

$$T_{\rm ev} \simeq \left(\frac{9 g_*(T_{\rm BH})}{10240}\right)^{\frac{1}{4}}\left(\frac{M_{\rm P}^5}{m_{\rm in}^3}\right)^{\frac{1}{2}}, \tag{6}$$

where $M_{\rm P}$ denotes the reduced Planck mass.

[2]Since our primary motive is to explore the effect of PBHs on dark radiation, in this work we remain agnostic about the formation mechanism of PBHs. PBHs with our desired mass range and initial energy density can be formed through several mechanisms, say from inflationary perturbations [33–35], Fermi-ball collapse [36], loop quantum gravity [37], etc.

For the early Universe to be black hole dominated, the initial energy density of a PBH should satisfy [21]

$$\beta \geq \beta_{\rm crit} \equiv 2.5\times 10^{-14}\gamma^{-\frac{1}{2}}\left(\frac{M_{\rm BH}(T_{\rm in})}{10^8\ {\rm g}}\right)^{-1}\left(\frac{\epsilon(M_{\rm BH}(T_{\rm in}))}{15.35}\right)^{\frac{1}{2}}. \tag{7}$$

Since PBH evaporation produces all particles, including radiation that can disturb the successful predictions of BBN, we require $T_{\rm ev} > T_{\rm BBN} \simeq 4$ MeV. This can be translated into an upper bound on the PBH mass. On the other hand, a lower bound on PBH mass can be obtained from the CMB bound on the scale of inflation [40]: $H_I \equiv H(T_{\rm in}) \leq 2.5\times 10^{-5} M_{\rm P}$, where $H(T_{\rm in}) = \frac{1}{2t_{\rm in}}$ with $t(T_{\rm in}) \propto m_{\rm in}$. Using these BBN and CMB bounds together, we have a window[3] for allowed initial mass for an ultralight PBH that reads $0.1\ {\rm g} \lesssim m_{\rm in} \lesssim 4\times 10^8$ g. We consider this allowed mass range of an ultralight PBH in the context of dark radiation. For simplicity, we consider a monochromatic mass function of PBHs implying that all PBHs have identical masses. Additionally, the PBHs are assumed to be of Schwarzschild type without any spin and charge.

Now, if there exist any light BSM degrees of freedom or dark radiation, they can be produced directly from evaporating PBHs, contributing to the effective number of relativistic degrees of freedom $\rm N_{eff}$ defined as

$$\rm N_{eff} = \frac{8}{7}\left(\frac{11}{4}\right)^{4/3}\left(\frac{\rho_R - \rho_\gamma}{\rho_\gamma}\right), \tag{8}$$

where ρ_R, ρ_γ denote total radiation and photon densities, respectively. In order to track the evolution of the energy densities, we need to consider the following set of Boltzmann equations [21]:

$$\frac{d\rho_{\rm BH}}{da} + 3\frac{\rho_{\rm BH}}{a} = \frac{1}{M_{\rm BH}}\frac{dM_{\rm BH}}{da}\rho_{\rm BH}, \tag{9}$$

$$aH\frac{d\rho_R}{da} + 4H\rho_R = -\frac{\epsilon_{\rm R}(M_{\rm BH})}{\epsilon(M_{\rm BH})}\frac{aH}{M_{\rm BH}}\frac{dM_{\rm BH}}{da}\rho_{\rm BH}, \tag{10}$$

$$a\frac{d\rho_X^{\rm BH}}{da} + 4\rho_X^{\rm BH} = -\frac{\epsilon_X(M_{\rm BH})}{\epsilon(M_{\rm BH})}\frac{a}{M_{\rm BH}}\frac{dM_{\rm BH}}{da}\rho_{\rm BH}. \tag{11}$$

Here, $\rho_X^{\rm BH}$ denotes energy density of a light species X produced solely from the evaporation of PBHs. The ϵ_R and ϵ_X are the evaporation functions of SM particles and X species, respectively. The combined evaporation function is denoted by $\epsilon = \epsilon_R + \epsilon_X$. The Hubble parameter H entering in the above equations is given by

$$H = \sqrt{\frac{\rho_{\rm BH} + \rho_{\rm SM} + \rho_X}{3M_{\rm P}^2}}. \tag{12}$$

Since entropy is not conserved due to PBH evaporation, we track the evolution of the thermal bath separately through the equation given by

$$\frac{dT}{da} = -\frac{T}{\Delta}\left(\frac{1}{a} + \frac{\epsilon_{\rm SM}(M_{\rm BH})}{\epsilon(M_{\rm BH})}\frac{1}{M_{\rm BH}}\frac{dM_{\rm BH}}{da}\frac{\rho_{\rm BH}}{4(\rho_{\rm SM}+\rho_X)}\right), \tag{13}$$

where

$$\Delta = 1 + \frac{T}{3g_{*s}(T)}\frac{dg_{*s}(T)}{dT}. \tag{14}$$

The extrarelativistic degrees of freedom $\Delta \rm N_{eff}$ is defined as

$$\Delta \rm N_{eff} = \frac{\rho_X(T_{\rm eq})}{\rho_{\nu_L,1}(T_{\rm eq})}. \tag{15}$$

Here $\rho_{\nu_L,1}(T_{\rm eq})$ denotes the energy density of one species of SM neutrinos at the time of matter-radiation equality. In terms of energy densities at the time of PBH evaporation, the above expression turns out to be [21]

$$\Delta \rm N_{eff}^{BH} = \left\{\frac{8}{7}\left(\frac{4}{11}\right)^{-\frac{4}{3}} + \rm N_{eff}^{SM}\right\} \times \frac{\rho_{\rm X}(T_{\rm ev})}{\rho_{\rm R}(T_{\rm ev})}\left(\frac{g_*(T_{\rm ev})}{g_*(T_{\rm eq})}\right)\left(\frac{g_{*s}(T_{\rm eq})}{g_{*s}(T_{\rm ev})}\right)^{\frac{4}{3}}, \tag{16}$$

where $\rm N_{eff}^{SM} = 3.044$ and $\rho_X(T_{\rm ev}), \rho_R(T_{\rm ev})$ denote the energy density of species X and SM after PBH evaporation, respectively. The relativistic degrees of freedom in energy and entropy densities are denoted by g_* and g_{*s}, respectively.

Now, in the case when a PBH dominates the energy density of the Universe at some epoch, Eq. (16) simplifies into

$$\Delta \rm N_{eff}^{BH} = 13.714 \times \frac{\epsilon_X(M_{\rm BH})}{\epsilon(M_{\rm BH})}\frac{g_*(T_{\rm ev})}{g_{*s}(T_{\rm ev})^{\frac{4}{3}}}. \tag{17}$$

From the above equation, we can see that $\Delta \rm N_{eff}$ remains constant for those values of PBH mass for which PBHs evaporate before the electroweak scale since g_*, g_{*s} remains constant at high temperatures. As we keep on increasing the PBH mass further, $\Delta \rm N_{eff}$ keeps on increasing. In the left panel of Fig. 1, we show the variation of $\Delta \rm N_{eff}$ with the initial PBH mass $m_{\rm in}$, for three different types of DR, which

[3]The range of PBH masses in this window remains typically unconstrained [30].

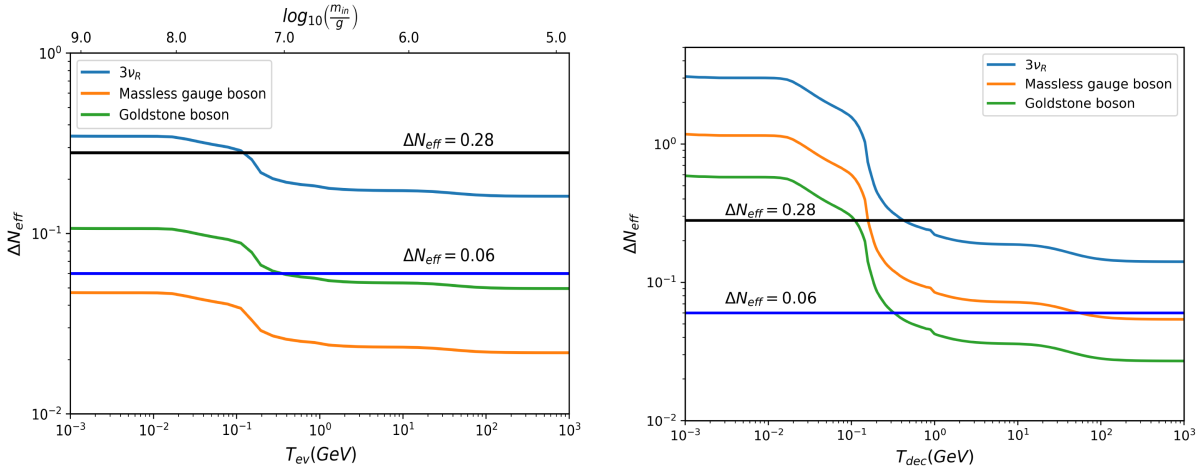

FIG. 1. Left: variation of nonthermal contribution to ΔN_{eff} coming from a PBH, with T_{ev} (or m_{in}) for different species. Right: variation of thermal contribution to ΔN_{eff} with T_{dec} for different species.

include the right chiral part of Dirac active neutrinos ν_R, the massless gauge boson (MGB), and the Goldstone boson (GB). The current 2σ bound from Planck 2018 [41] and the future sensitivity of CMB-S4 [16] is also shown in the same figure.

III. THERMALIZED DARK RADIATION IN THE PRESENCE OF A PBH

If we consider the extrarelativistic species to have interactions with the SM bath, ΔN_{eff} would receive a thermal contribution that depends on the temperature at which the thermal species decouple from the bath, namely, T_{dec}. It can be written as [42]

$$\Delta N_{eff}^{th} = 0.0267 \times f n_X g_X \left(\frac{106.75}{g_{*s}(T_{dec})}\right)^{4/3}, \quad (18)$$

where g_X, n_X is the internal spin degree of freedom of X and number of different species of type X, respectively. f takes the value of $7/8$ for fermions and 1 for bosons. T_{dec} denotes the decoupling temperature of the thermalized species. In the right panel of Fig. 1, we show the corresponding ΔN_{eff} by considering DR to be of thermal origin only. The x axis denotes the decoupling temperature T_{dec} of DR from the thermal bath. As expected, a lower decoupling temperature leads to a larger contribution to ΔN_{eff}.

As we will see, in the presence of a PBH, the total contribution to ΔN_{eff} from thermalized DR is decided by the interplay between the thermal and the nonthermal contribution. Interestingly, the total contribution depends on when the PBH evaporates relative to the decoupling temperature of the thermalized species. Depending on the initial fractional energy density (β) and the initial mass (m_{in}) of a PBH at the time of formation, we can broadly divide our study into two categories: (a) a PBH dominates the energy density of the Universe at some epoch, and (b) a PBH never dominates the energy density of the Universe. These two possibilities lead to different observational consequences, which we discuss below.

A. PBH domination

The evaporation of a PBH will produce all the SM particles along with DR. In the hybrid scenario considered here, DR can be produced gravitationally from a PBH as well as from the SM bath by virtue of nonstandard DR-SM interactions. Therefore, we can think of the total contribution to the extra number of relativistic species ΔN_{eff} as the contribution from DR emitted from a PBH and the already existing thermal counterpart, which was thermalized followed by decoupling from the thermal bath.

The decoupling temperature of extra light species X depends on its coupling with SM particles. A smaller value of coupling can lead to an early decoupling. In such a scenario, the duration between decoupling and PBH evaporation can be quite long. Thus, to begin with, we neglect the interaction between the decoupled X and X produced from a PBH. So, both decoupled and light species from a PBH can be treated as different species while considering their individual contribution to ΔN_{eff}. In a follow-up section, we explicitly consider a specific type of DR, namely, Dirac-type active neutrinos with four-fermion-type interactions of right chiral part with the SM and study the validity of this assumption. On the other hand, for a larger value of DR-SM coupling, the PBH evaporation can occur much before the decoupling of light species X. In that case, the emitted X from a PBH will be thermalized completely with the SM bath, and both emitted and preexisting thermal X will behave as a single species.

Here, we make an estimate of ΔN_{eff} in the two limits discussed above. The evaporation temperature of a PBH is connected to the initial PBH mass m_{in} through Eq. (6). Assuming that the species X decouples at the same

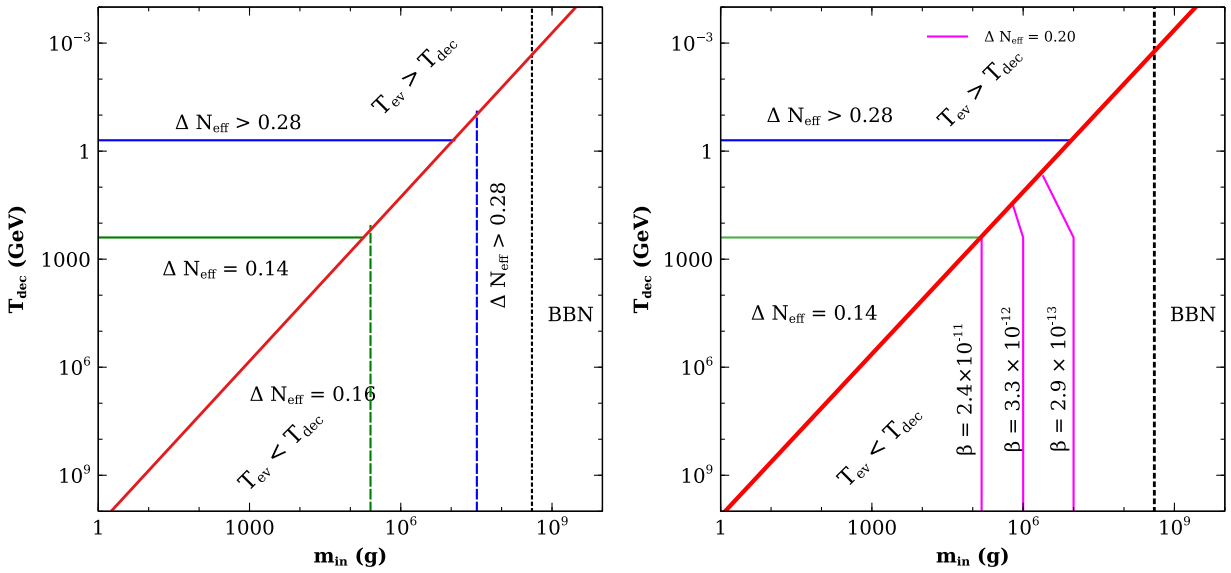

FIG. 2. $\Delta N_{\rm eff}$ contours in the plane of initial PBH mass versus decoupling temperature. Here, we consider the extra light species X to be ν_R. The left side is for the case where PBHs dominate the energy density at the time of evaporation, whereas on the right, PBH energy density is always less than that of radiation. The black vertical dashed line indicates the upper bound on PBH mass from the BBN limit.

temperature as PBH evaporation, we can draw the solid red line in Fig. 2 corresponding to $T_{\rm ev} = T_{\rm dec}$. Now, depending upon the values of its coupling with SM and $m_{\rm in}$, we can have the two different scenarios, i.e., either $T_{\rm ev} > T_{\rm dec}$ (above the red line) or $T_{\rm ev} < T_{\rm dec}$ (below the red line). We discuss the dynamics for these two cases below.

1. PBH evaporation before decoupling of thermalized DR

We first consider the scenario where the PBH evaporates earlier than the decoupling of thermalized species X. In such a case, the species X produced from PBH evaporation will also get thermalized. Therefore, the contribution to $\Delta N_{\rm eff}$ comes only from the thermalized X and is given by Eq. (18). For example, if X is considered to be the right chiral part of Dirac active neutrinos, this equation reduces to

$$\Delta N_{\rm eff} \simeq 0.027 \times 2 \times 3 \times \frac{7}{8}\left(\frac{106.75}{g_*(T_{\rm dec})}\right)^{4/3} \simeq 0.14175 \times \left(\frac{106.75}{g_*(T_{\rm dec})}\right)^{4/3}. \tag{19}$$

Thus, $\Delta N_{\rm eff}$ becomes independent of $m_{\rm in}$. For decoupling temperature $T_{\rm dec} \lesssim 500$ MeV, $\Delta N_{\rm eff}$ is more than 0.28, the current Planck bound at 2σ level. This is indicated by the region above the solid blue line in Fig. 2. A larger decoupling temperature reduces the contribution to $N_{\rm eff}$. Note that this also requires a smaller value of PBH mass to make sure that a PBH evaporates earlier compared to the decoupling epoch. Above a certain value of $T_{\rm dec}$, the contribution to $\Delta N_{\rm eff}$ saturates at a value of 0.14, indicated by the triangular region between solid green and solid red lines of Fig. 2.

2. PBH evaporation after decoupling of thermalized DR

Next, we consider the scenario where a PBH evaporates after the thermal decoupling of species X. In this case, $\Delta N_{\rm eff}$ can, in principle, get contributions from both sources. We can write

$$\Delta N_{\rm eff} = \Delta N_{\rm eff}^{\rm BH} + \Delta N_{\rm eff}^{\rm th}, \tag{20}$$

where the first term on the right-hand side (rhs) denotes the contribution from a PBH and the second term indicates the thermal contribution. Now, for PBH domination, evaporation of a PBH will lead to entropy injection to the thermal bath. Thus, the thermal contribution from X to $\Delta N_{\rm eff}$ gets diluted. Taking into account the effect of dilution, the above equation for Dirac active neutrinos can be written as

$$\Delta N_{\rm eff} = 0.772\,\frac{g_*(T_{\rm ev})}{(g_{*s}(T_{\rm ev}))^{4/3}} + 0.14175 \times \left(\frac{106.75}{g_*(T_{\rm dec})}\right)^{4/3}\xi^{-4/3}, \tag{21}$$

where the parameter ξ quantifies decrease in $\Delta N_{\rm eff}$ due to entropy dilution. It can be written as the ratio of the comoving entropy density at PBH evaporation $(T_{\rm ev})$ to that at thermal decoupling of X $(T_{\rm dec})$

$$\xi = \frac{S_{\rm ev}}{S_{\rm dec}} = \frac{g_{*s}(T_{\rm ev})a^3(T_{\rm ev})T_{\rm ev}^3}{g_{*s}(T_{\rm dec})a^3(T_{\rm dec})T_{\rm dec}^3}. \tag{22}$$

Without any entropy injection, conservation of entropy gives $\xi = 1$. For entropy injection due to PBH evaporation, we have $\xi > 1$. It turns out that for PBH-dominated region, $\xi \gg 1$, diluting the contribution from thermal ν_R or X, in general. Thus, one can safely neglect the second term on the rhs of Eq. (20). Hence, only the X from a PBH will contribute to $\Delta N_{\rm eff}$. PBH mass greater than around 4×10^7 g leads to $\Delta N_{\rm eff}$ greater than the Planck 2σ bound, as shown earlier (cf. left panel of Fig. 1).

B. Radiation domination

If the ratio of the initial energy density of PBH to that of radiation energy density is less than $\beta_{\rm crit}$, the early Universe remains dominated by radiation only. Similar to the PBH-dominated universe, we can also have the same two scenarios, namely, $T_{\rm ev} > T_{\rm dec}$ and $T_{\rm ev} < T_{\rm dec}$. The solid red line in the right panel of Fig. 2 corresponds to $T_{\rm dec} = T_{\rm ev}$. We discuss the two scenarios corresponding to either side of this solid red line below.

1. PBH evaporation before decoupling of thermalized DR

Similar to the case of PBH domination, here the thermal contribution is the only contributing factor to $\Delta N_{\rm eff}$. Hence, the region and bounds are same as that of PBH domination, as already discussed in Sec. III A 1.

2. PBH evaporation after decoupling of thermalized DR

Here, the total contribution to $\Delta N_{\rm eff}$ can be written in the form of Eq. (20), with the nonthermal contribution $\Delta N_{\rm eff}^{\rm BH}$ given by Eq. (16). $\Delta N_{\rm eff}^{\rm BH}$ is evaluated by solving the Boltzmann equations (9)–(11). Unlike the case of PBH domination, here the contribution from the thermalized DR cannot be neglected as the entropy injection is negligible (i.e., $\xi \sim 1$) for $\beta < \beta_{\rm crit}$. Hence, $\Delta N_{\rm eff}$ will bear contribution from both thermalized as well as PBH generated DR. Also, for PBH domination, $\Delta N_{\rm eff}^{\rm BH}$ is independent of the parameter β, whereas in the present scenario β plays a significant role. The role of β can be seen from the magenta colored lines shown in the right panel plot of Fig. 2. The magenta colored lines denote a total $\Delta N_{\rm eff} = 0.20$. As the initial mass of PBH increases, its contribution to $\Delta N_{\rm eff}$ also increases. As a result, one needs to reduce the value of β to get the same $\Delta N_{\rm eff}$. Let us consider the magenta line with $m_{\rm in} = 10^7$ g. The straight vertical portion of the line indicates a thermal contribution of 0.14 and a PBH contribution of 0.06. The contribution from PBH can be set to the required value by adjusting β. Decreasing $T_{\rm dec}$ in the right panel plot up to ∼200 GeV leads to no changes in the thermal contribution as g_{*s} remain constant, giving a constant contribution to $\Delta N_{\rm eff}^{\rm th}$. Decreasing $T_{\rm dec}$ below ∼200 GeV, the thermal contribution increases due to the reasons discussed earlier. So, one requires a smaller contribution of $\Delta N_{\rm eff}^{\rm BH}$ in order to maintain a total contribution of 0.20. This can be done by either decreasing PBH mass or by decreasing β. Here we decrease the PBH mass, keeping β constant. This leads to the bending of magenta lines for $T_{\rm dec} < 200$ GeV.

C. Summary of results

Now let us look at the combined results of PBH and radiation domination in the β-$m_{\rm in}$ plane. In the PBH-dominated case, the magenta-shaded region in Fig. 3 shows the portion of parameter space where $\Delta N_{\rm eff} > 0.28$, corresponding to PBH initial mass $m_{\rm in} \gtrsim 4 \times 10^7$ g (cf. blue dashed contour of left panel plot in Fig. 2). Now, this constraint is only valid if ν_R (or DR, in general) decouples from the bath before PBH evaporation, i.e., if $T_{\rm dec} >$ 150 MeV (intersection of the blue dashed contour with the solid red line in the left panel plot of Fig. 2). If ν_R decouples after PBH evaporation, then $\Delta N_{\rm eff}$ will bear contribution from thermalized ν_R (existing thermal $\nu_R + \nu_R$ from PBH that will also get thermalized). In such a case, no constraint on the PBH parameters β or $m_{\rm in}$ can be obtained, since the contribution is purely thermal.

In the radiation-dominated region, if the thermalized ν_R decouples earlier, then even for very small β, one expects a minimum contribution of $\Delta N_{\rm eff}^{\rm th} = 0.14$ to $\Delta N_{\rm eff}$. For example, let us fix $T_{\rm dec} \approx 35$ GeV. So, for PBH mass greater than $\sim 7 \times 10^5$ g, the decoupling of ν_R occurs before PBH evaporation. The thermal contribution to $\Delta N_{\rm eff}$ is about ≈0.17. So, if the PBH contribution to $\Delta N_{\rm eff}$ is more than 0.11, the total $\Delta N_{\rm eff}$ would exceed 0.28. The blue-shaded region in Fig. 3 denotes the area for which $\Delta N_{\rm eff} > 0.28$. Note that there is a discontinuity between

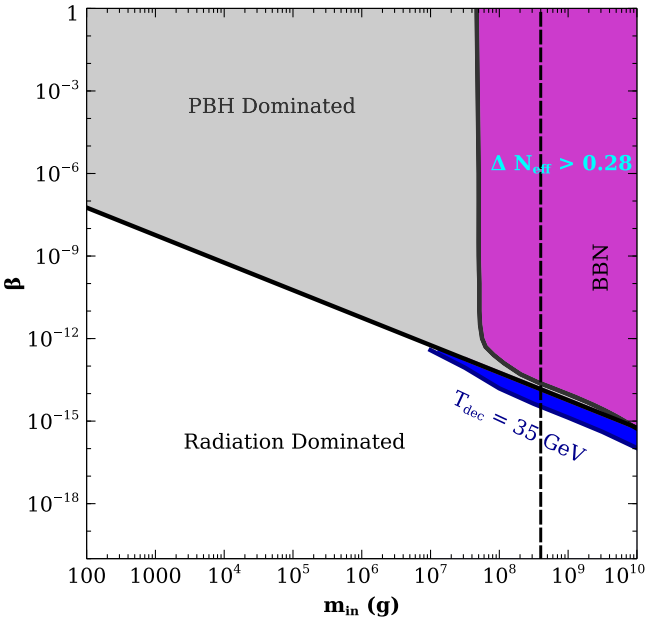

FIG. 3. $\Delta N_{\rm eff}$ contours in the β-$m_{\rm in}$ plane. The magenta and blue region are the portion for PBH and radiation domination, respectively, where $\Delta N_{\rm eff} > 0.28$. The black vertical dashed line indicates the upper bound on PBH mass from BBN limit.

the magenta- and blue-shaded regions. This is because we have assumed that, in the PBH-dominated era, the thermal contribution to $\Delta N_{\rm eff}$ will be totally diluted away due to subsequent PBH evaporation and hence can be neglected. However, in the vicinity of the solid red line, i.e., $\beta \sim \beta_{\rm crit}$, the dilution would be smaller, leading to a non-negligible thermal contribution that should be counted for. At the same time, for the radiation-dominated case, we have assumed no entropy dilution for the thermal contribution, which is not completely true in the vicinity of $\beta \sim \beta_{\rm crit}$. This is due to the fact that even a subdominant but sizable abundance of PBHs can lead to some entropy dilution, howsoever small. All these intricacies will be taken care of when we explicitly solve the relevant Boltzmann equations by properly taking into account the entropy dilution factor near the transition region from PBH to radiation domination, which we discuss below.

We perform a numerical analysis to evaluate the total contribution to $\Delta N_{\rm eff}$. For this purpose, we use the publicly available code FRISBHEE [26] to calculate the nonthermal contribution $\Delta N_{\rm eff}^{\rm BH}$ and to properly include the entropy dilution factor [cf. Eq. (22)], which goes into the calculation of the thermal contribution $\Delta N_{\rm eff}^{\rm th}$. For illustrative purposes, we consider the DR or the extra light species X to be of three types, namely, (i) ν_R, (ii) the Goldstone boson, and (iii) the massless gauge boson.

1. Dirac neutrino

Here, we consider three species of ν_R as the extra light degrees of freedom, as in usual Dirac active neutrino scenarios. In Fig. 4, we show the total contribution to $\Delta N_{\rm eff}$ in the $m_{\rm in}$-β plane for four different subcases. In the top left panel, we show the results where ν_R is produced purely from PBH due to negligible interactions with the SM bath. The black dashed contour corresponds to $\Delta N_{\rm eff} = 0.28$, the maximum allowed by Planck 2018 data at 2σ level. This plot can be taken as a reference to compare

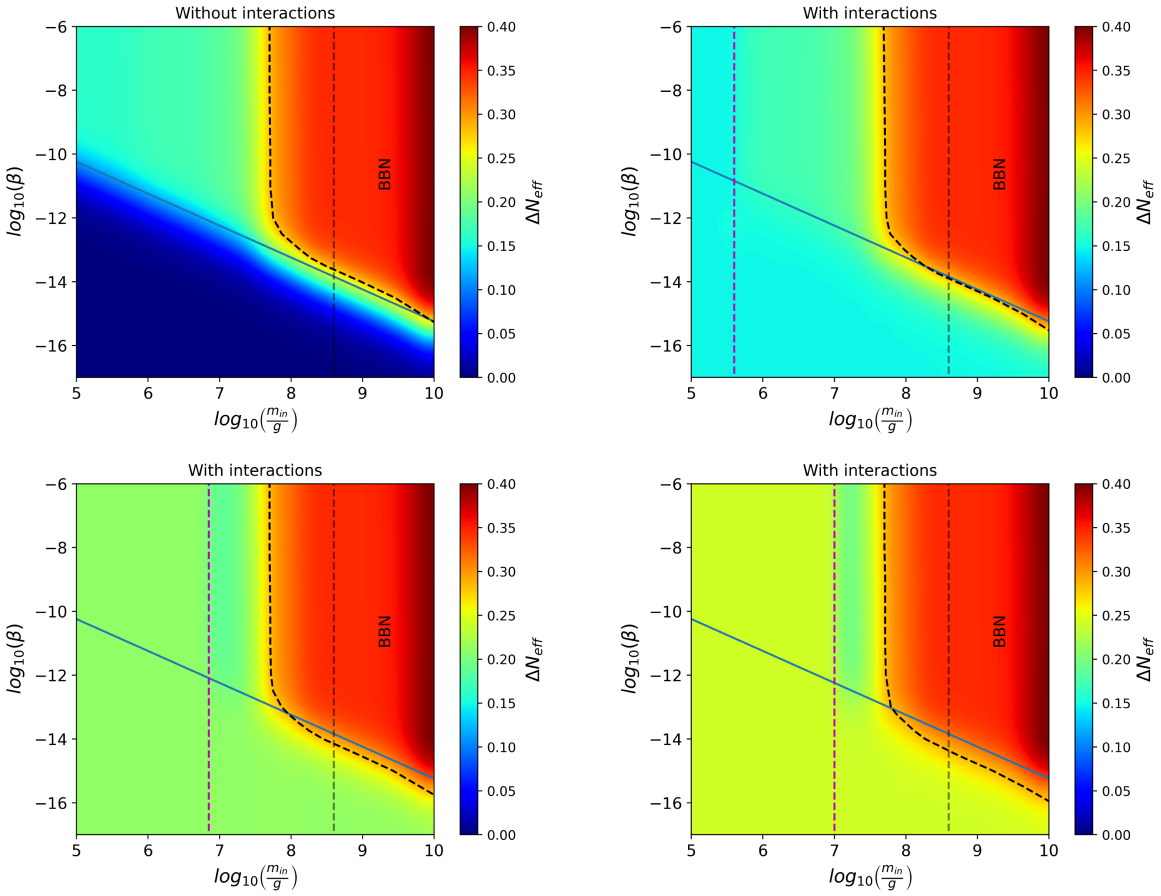

FIG. 4. Dirac neutrino: Variation of $\Delta N_{\rm eff}$ in the $m_{\rm in}$ versus β plane for four different scenarios related to Dirac neutrinos: without any extra interactions of ν_R (top left), with interactions giving $\Delta N_{\rm eff}^{\rm th} = 0.14$, $T_{\rm dec} = 100$ GeV, (top right), $\Delta N_{\rm eff}^{\rm th} = 0.21$, $T_{\rm dec} = 1$ GeV (bottom left) and $\Delta N_{\rm eff}^{\rm th} = 0.24$, $T_{\rm dec} = 850$ MeV (bottom right), respectively. The regions to the right of the black dashed line indicate $\Delta N_{\rm eff} > 0.28$ ruled out by Planck 2018 data at 2σ level. The dashed blue vertical line separates the regions $T_{\rm dec} < T_{\rm ev}$ and $T_{\rm dec} > T_{\rm ev}$ (not applicable to the top left figure due to no DR-SM interactions). The gray vertical dashed line indicates the upper bound on PBH mass from BBN limit.

the results in the presence of extra interactions. In the top right panel of Fig. 4, we show the results when the contribution from thermal ν_R is $\Delta N_{\rm eff}^{\rm th} \sim 0.147$. For this particular value of $\Delta N_{\rm eff}^{\rm th}$, the decoupling temperature should be $T_{\rm dec} \gtrsim 100$ GeV corresponding to PBH mass $m_{\rm in} \sim 4 \times 10^5$ g. PBH masses greater than $\sim 4 \times 10^5$ g will evaporate later, satisfying $T_{\rm ev} < T_{\rm dec}$. The vertical dashed line distinguishes these two regions. For $\beta \gg \beta_{\rm crit}$, there is no change on the Planck 2018 bound compared to the results without interactions, as the contribution of thermally decoupled species is negligible because of entropy dilution from PBH evaporation. However, near $\beta \sim \beta_{\rm crit}$, i.e., the transition region between PBH and radiation domination, we can see a decrease, albeit small, in the values of β required to produce the same value of $\Delta N_{\rm eff}$ as in the case without interactions. This is because, near the boundary of the transition region, the effect of the thermal contribution starts appearing; hence we need a lower value of β such that the nonthermal contribution $\Delta N_{\rm eff}^{\rm BH}$ decreases, resulting in a similar value of the total $\Delta N_{\rm eff}$. This explains the slight lowering of the black dashed contour corresponding to $\Delta N_{\rm eff} = 0.28$. Note that the minimum contribution of the thermal species is 0.147, which is visible as we depart from the transition region. This is in sharp contrast to the results without interactions, where the value of $\Delta N_{\rm eff}$ fades away to zero as we move deeper into the radiation domination ballpark. In the bottom panel, we have $\Delta N_{\rm eff}^{\rm th} = 0.21$ (left) and 0.24 (right). Because of the higher values of $\Delta N_{\rm eff}^{\rm th}$, and hence a lower decoupling temperature, the dashed vertical line shifts to the right, corresponding to higher values of PBH mass (lower $T_{\rm ev}$). Here, the change in the transition region is more apparent, due to a decrease in the contribution from the PBH, namely, $\Delta N_{\rm eff}^{\rm BH}$. We can see that, for $\Delta N_{\rm eff}^{\rm th} = 0.24$, much more parameter space near the transition region is ruled out by current Planck 2018 data compared to that in the case without interactions (cf. top left panel of Fig. 4).

2. Goldstone boson

Let us consider the extra light species to be a Goldstone boson, a massless scalar. From Fig. 1 discussed before, we can see that the maximum contribution of Goldstone boson produced solely from an evaporating PBH to $\Delta N_{\rm eff}$ is 0.10, which is below the Planck 2018 limit. However, it comes under the sensitivity of future experiments like CMB-S4. The top left panel of Fig. 5 shows the bound on $\Delta N_{\rm eff}$ without any interaction. Unlike the case of ν_R, here the region to the right of the black dashed contour represents $\Delta N_{\rm eff} > 0.06$, the CMB-S4 sensitivity, as Planck 2018 data do not rule out any region of the parameter space at 2σ level. The top right panel and the bottom panel show the corresponding bounds with interactions between GB and SM. In the top right panel, the decoupling temperature is $T_{\rm dec} = 100$ GeV and in the bottom panel, the decoupling temperature is $T_{\rm dec} = 1$ GeV. These correspond to $\Delta N_{\rm eff}^{\rm th} = 0.028$ and 0.042, respectively. Similar to the previous situation, a lower decoupling temperature gives a stronger constraint on the β versus $m_{\rm in}$ plane.

3. Massless gauge boson

From Fig. 1 discussed earlier, it can be seen that, in the absence of a PBH, the contribution of thermalized massless gauge boson to $\Delta N_{\rm eff}$ is within the future CMB-S4 sensitivities for decoupling temperature $T_{\rm dec} \lesssim 100$ GeV. As a result, a wide range of interactions of MGBs with the SM for which $T_{\rm dec} \lesssim 100$ GeV can be probed by future CMB experiments like CMB-S4 (cf. right panel of Fig. 1). On the other hand, if a PBH dominates in the early Universe, the contribution to $\Delta N_{\rm eff}$ always remains beyond the reach of future sensitivities, as shown in Fig. 1 (left panel). Thus, even if CMB-S4 rules out large coupling between MGBs and SM, which would produce large $\Delta N_{\rm eff}$, such large couplings (or, equivalently, lower $T_{\rm dec}$) would still be allowed if we consider PBH domination in the early Universe. This would be possible if we consider that the PBH evaporates after the decoupling of MGBs and sufficiently dilutes the thermal contribution.

IV. AN EXAMPLE: THERMALIZED DIRAC NEUTRINO IN THE PRESENCE OF PBH

In the previous sections, we have studied the consequence of thermalized DR in the presence of PBH, while considering different examples of DR as well as PBH parameters, corresponding to both PBH and radiation domination in the early Universe. However, we discussed our results only in terms of decoupling temperatures of thermalized DR while being agnostic about the type of interactions with the SM bath. In this section, we consider a specific type of DR, namely, light Dirac neutrinos and discuss our results for effective four-fermion-type interactions with the SM parametrized by the coupling parameter $G_{\rm eff}$. Enhancement of $\Delta N_{\rm eff}$ in Dirac neutrino models (without PBHs) have been studied in several recent works [42–57].

The SM extended by three right-handed singlet Dirac neutrinos with Yukawa interactions $\mathcal{L}_Y = -Y_\nu^{ab} \overline{\ell^a_L} \tilde{\Phi} \nu_{bR}$ can explain tiny neutrino mass of $\mathcal{O}(\text{eV})$, with $Y_\nu \sim 10^{-12}$ as a result of electroweak symmetry breaking induced by the SM Higgs doublet Φ. However, such small interactions cannot thermalize the ν_R. Because of the smallness of Yukawa coupling, the nonthermal or freeze-in contribution to $\Delta N_{\rm eff}$ from ν_R also remains negligible [49]. Thermalization of ν_R may be possible in the presence of nonstandard interactions, which we consider to be of four-fermion-type interactions with the SM neutrinos ν_L [46] (see the Appendix for details). This allows us to work in a model-independent manner while constraining the effective interactions as well as PBH parameters. The total

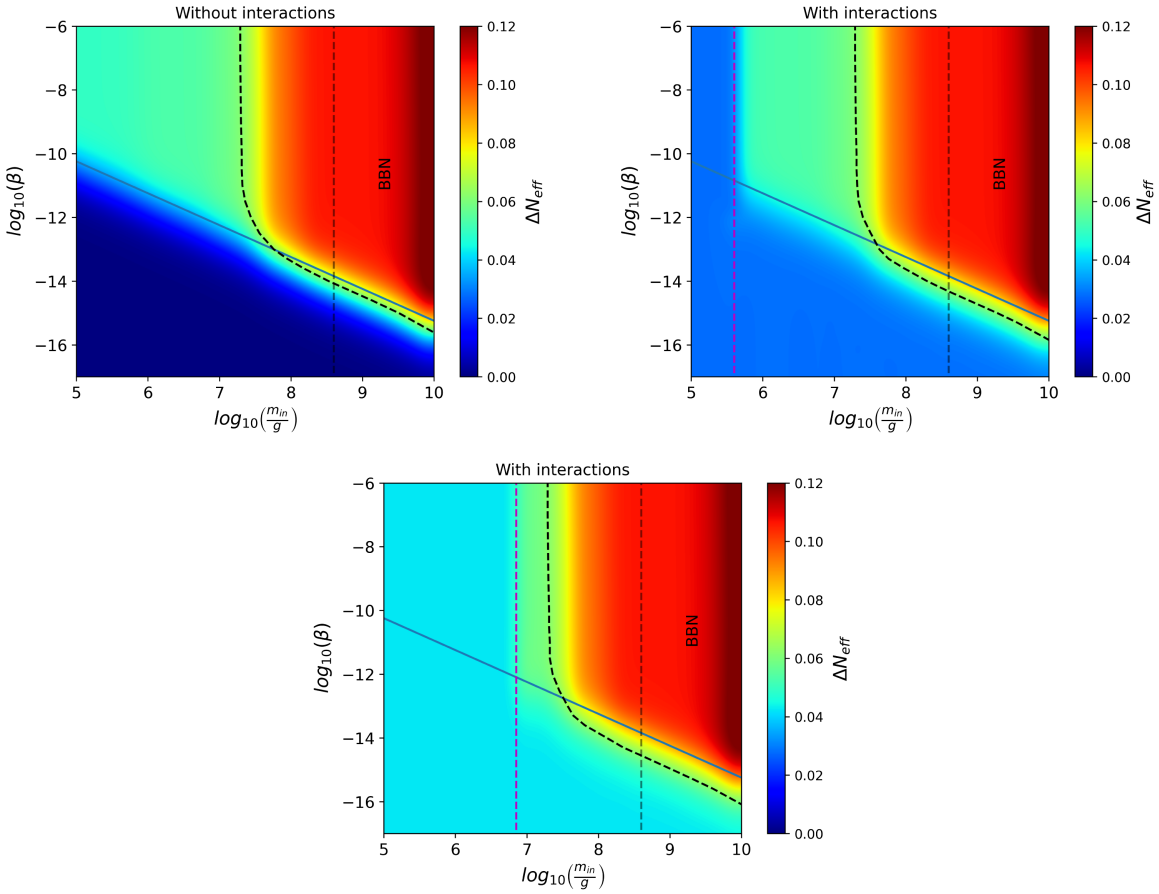

FIG. 5. Goldstone boson: Variation of ΔN_{eff} in the m_{in} versus β plane for three different scenarios related to the Goldstone boson: without any extra interactions (top left), with interactions giving $\Delta N_{eff}^{th} = 0.028$, $T_{dec} = 100$ GeV (top right), and $\Delta N_{eff}^{th} = 0.042$, $T_{dec} = 1$ GeV (bottom), respectively. The regions to the right of the black dashed contour indicate $\Delta N_{eff} > 0.06$, the CMB-S4 sensitivity. The dashed blue vertical line separates the regions $T_{dec} < T_{ev}$ and $T_{dec} > T_{ev}$. The gray vertical dashed line indicates the upper bound on PBH mass from BBN limit.

interaction rate of ν_R arising from such four-fermion operators can be written as

$$\Gamma = n_R^{eq}\langle\sigma v\rangle \simeq \frac{3}{4}\frac{\zeta(3)}{\pi^2} 2T^3 \frac{1}{4\pi} 4(3.151T)^2 G_{eff}^2, \quad (23)$$

where G_{eff} is given by

$$G_{eff}^2 = \frac{4}{3}(G_S - 12G_T)^2 + \frac{5}{12}(\tilde{G}_S - 2G_V)^2, \quad (24)$$

where $G_S, \tilde{G}_S, G_T, G_V$ are dimensionful couplings involved in different four-fermion operators involving ν_R and ν_L as shown in the Appendix. The equilibrium number density is denoted by n_R^{eq}. Comparing this interaction rate Γ with the Hubble rate of expansion [given by Eq. (12) and obtained by solving the Boltzmann equations (9)–(11)], we can find the decoupling temperature of ν_R. Note that the Hubble parameter contains contributions from both SM radiation and PBH, which can lead to a change in the ν_R decoupling temperature compared to the standard case without PBH.

With this, we redraw Fig. 2 by replacing T_{dec} in the y axis with the equivalent G_{eff}. The resulting plots are shown in Figs. 6 and 7 for PBH and radiation domination, respectively. In the left panel of Fig. 6, the coupling G_S is nonzero, while the rest (i.e., $G_T, \tilde{G}_S$ and G_V) are zero. In the right panel, G_T is nonzero and the rest are set to zero. For $G_{eff} \gtrsim 10^{-3} G_F$, with G_F being the Fermi coupling, the decoupling temperature of ν_R turns to be $\lesssim$500 MeV and ΔN_{eff} is more than 0.28. Similarly, below a certain value of coupling, $G_{eff} \sim 2 \times 10^{-7} G_F$, the contribution to ΔN_{eff} saturates at a value of 0.14. The corresponding parameter space is shown for the case of radiation domination in Fig. 7, which can be understood in a way analogous to the right panel of Fig. 2 discussed earlier.

Now, in order to check whether the right-handed neutrinos produced after PBH evaporation enters into thermal equilibrium with the SM bath, we calculate the interaction of ν_L present in the bath and nonthermal ν_R produced from PBH evaporation. Following [58], the

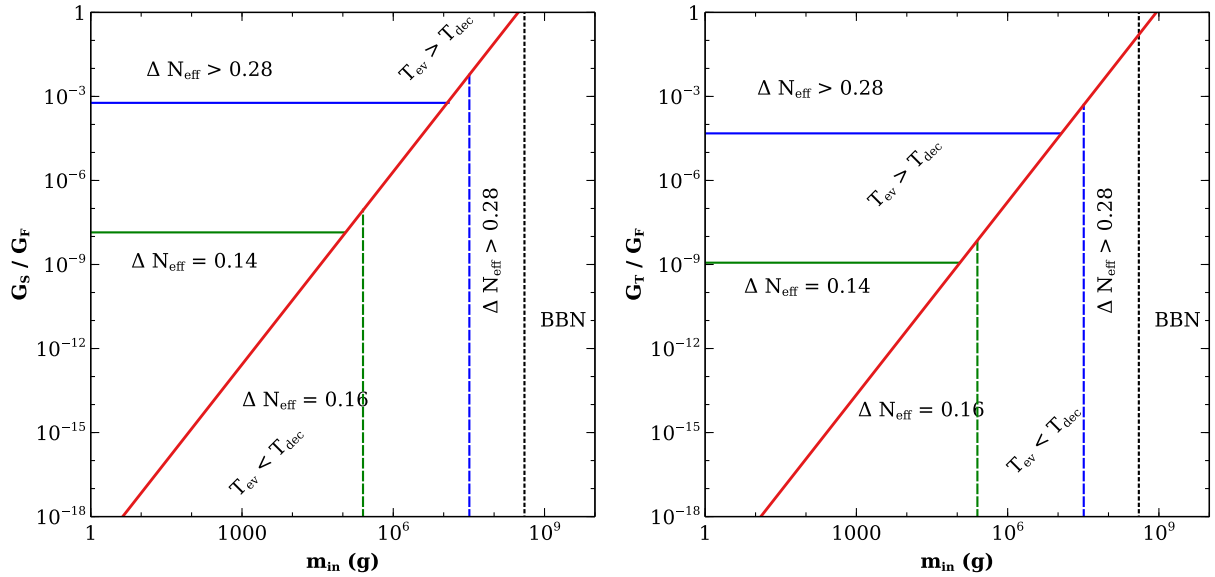

FIG. 6. $\Delta N_{\rm eff}$ contours in the plane of initial PBH mass versus the effective neutrino coupling for the case of PBH domination. Left: $G_T = \tilde{G}_S = G_V = 0$ with nonzero G_S. Right: $G_S = \tilde{G}_S = G_V = 0$ with nonzero G_T. The black vertical dashed line indicates the upper bound on PBH mass from BBN limit.

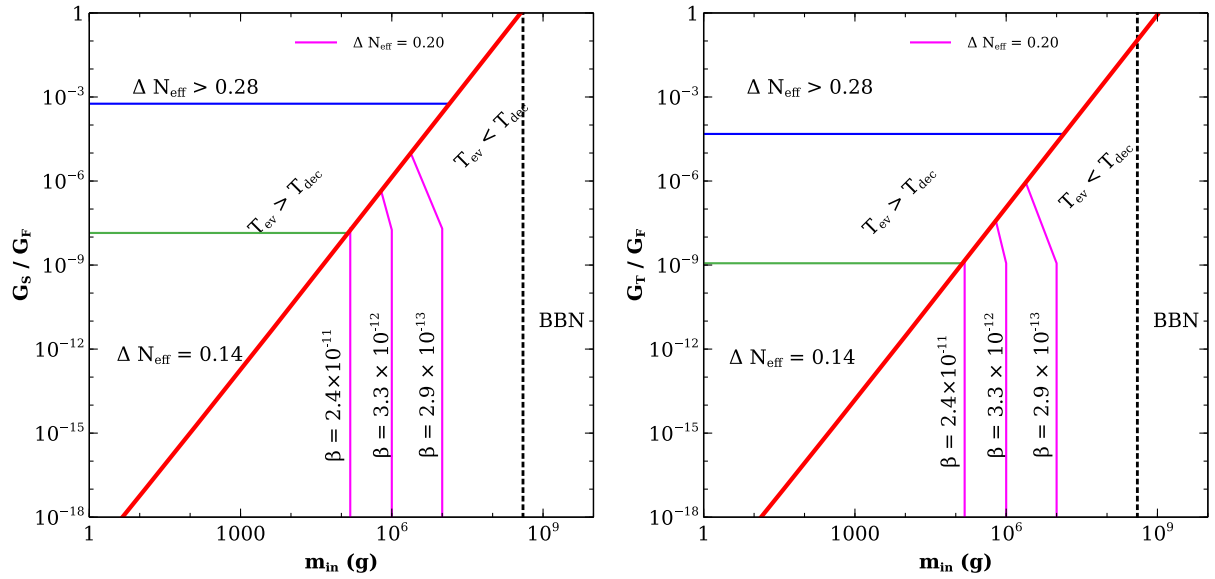

FIG. 7. $\Delta N_{\rm eff}$ contours in the plane of initial PBH mass versus the effective neutrino coupling for the case of radiation domination. Left: $G_T = \tilde{G}_S = G_V = 0$ with nonzero G_S Right: $G_S = \tilde{G}_S = G_V = 0$ with nonzero G_T. The black vertical dashed line indicates the upper bound on PBH mass from BBN limit.

thermal averaged cross section for two massless species having different temperatures is found to be

$$\langle \sigma v \rangle_{T_{\rm ev} T_{\rm BH}} = \frac{1}{32 (T_{\rm ev} T_{\rm BH})^{5/2}} \int_0^\infty \sigma s^{3/2} K_1 \left(\frac{\sqrt{s}}{\sqrt{T_{\rm ev} T_{\rm BH}}} \right) ds, \tag{25}$$

with K_1 being the modified Bessel function of order 1. For $\sigma = \frac{1}{4\pi} s G_{\rm eff}^2$, this gives

$$\langle \sigma v \rangle_{T_{\rm ev} T_{\rm BH}} = \frac{6}{\pi} G_{\rm eff}^2 T_{\rm ev} T_{\rm BH}. \tag{26}$$

Comparing the interaction rate corresponding to the above cross section with the Hubble rate leads to the thermalization condition

$$\frac{n_{\nu_L}^{\rm eq}(T_{\rm ev}) \langle \sigma v \rangle_{T_{\rm ev} T_{\rm BH}}}{H(T_{\rm ev})} = C \frac{6}{\pi} G_{\rm eff}^2 T_{\rm ev}^2 T_{\rm BH} = 1, \tag{27}$$

where $C = \frac{\frac{3}{4}\zeta(3) \times 2 \times \sqrt{45} \times M_{\rm P}}{\pi^2 \sqrt{4\pi^3 g_*(T_{\rm ev})}}$.

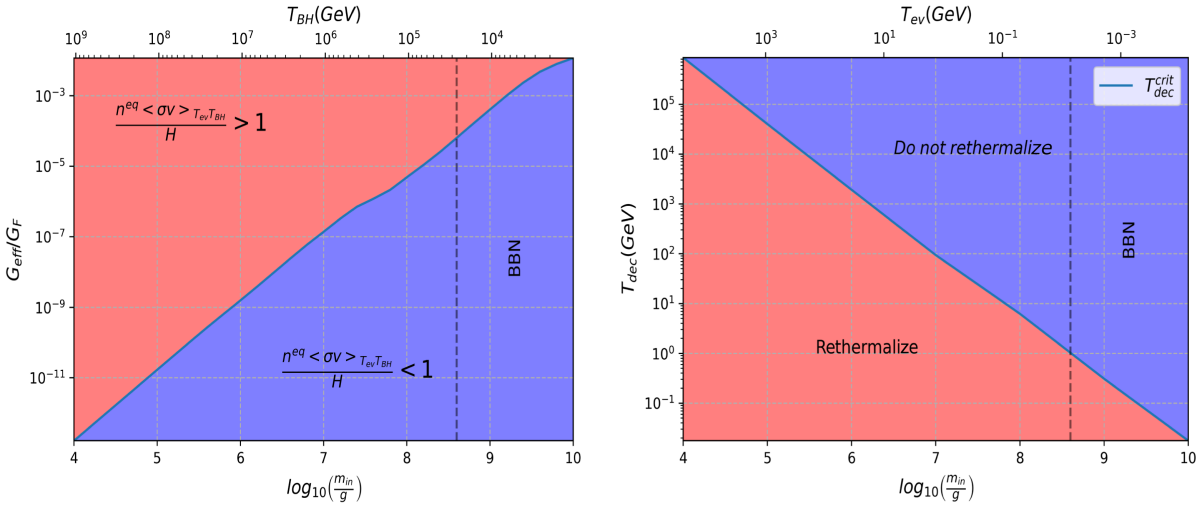

FIG. 8. Left: $m_{\rm in}$ versus $G_{\rm eff}/G_{\rm F}$ parameter space showing the possibility of rethermalization. The red (blue) colored region denotes the parameter space for which the PBH generated ν_R can (cannot) come into thermal equilibrium. Right: $m_{\rm in}$ versus $T_{\rm dec}$ parameter space showing the possibility of rethermalization. The red and blue colored regions have the same meaning as the ones on the left. The vertical dashed line indicates the upper bound on PBH mass from BBN limit.

Both $T_{\rm ev}$ and $T_{\rm BH}$ are functions of $m_{\rm in}$ as can be seen from Eqs. (6) and (3). In the left panel of Fig. 8, we show the parameter space in the $m_{\rm in}$-$G_{\rm eff}$ plane, where rethermalization of the PBH generated ν_R takes place (red shaded), along with the region that does not lead to such rethermalization (blue shaded). We can see that, for a fixed PBH mass, if $G_{\rm eff}$ is smaller than a particular critical value, the nonthermally generated ν_R from the PBH never thermalizes again with the bath. A smaller value of $G_{\rm eff}$ also implies a higher initial decoupling temperature of thermal ν_R. Hence, it is also possible to relate this critical value of $G_{\rm eff}$ below which rethermalization does not occur, with the initial decoupling temperature of ν_R. In the right panel of Fig. 8, we show the parameter space in the $m_{\rm in}$-$T_{\rm dec}$ plane, separating the region of rethermalization from the rest. For a particular PBH mass, a decoupling temperature higher than $T^{\rm crit}_{\rm dec}$ leads to the situation where ν_R from the PBH will never rethermalize with the bath.[4]

To summarize, Fig. 8 shows the constraints on the parameter space for which the ν_R produced from PBH evaporation will never rethermalize. Once we identify the parameter space where rethermalization occurs, the next step is to find the new $\Delta {\rm N}_{\rm eff}$ for these regions. However, this requires a careful treatment of complete Boltzmann equations to track the phase-space distribution function of evaporated ν_R, which is numerically expensive and out of the scope of the current work. Here, we assume that the new decoupling temperature of ν_R after rethermalization is $\sim T_{\rm ev}$ for a particular PBH mass. This can be justified by the fact that PBH generated ν_R, having a large initial energy and a sufficiently large interaction rate with the bath responsible for rethermalization, also suffer from instant dissipation of the energy to the bath. Because of this instant dissipation of energy, ν_R cannot maintain equilibrium for a longer period after rethermalization, leading to decoupling of ν_R once again at a temperature very close to $T_{\rm ev}$.

With this, it is possible to find new constraints on $G_{\rm eff}$ and $m_{\rm in}$. In the left panel of Fig. 9, constraints are shown in the $m_{\rm in}$-$G_{\rm eff}$ plane. The black dashed lines denote $\Delta {\rm N}_{\rm eff} = 0.28$. Taking into account rethermalization, it is possible to obtain a stronger constraint on $G_{\rm eff}/G_{\rm F}$. In the region, $T_{\rm dec} < T_{\rm ev}$, $\Delta {\rm N}_{\rm eff} > 0.28$ implies $G_{\rm eff}/G_{\rm F} \gtrsim 5 \times 10^{-4}$. However, in the rethermalization region, $G_{\rm eff}/G_{\rm F}$ up to $\sim 5 \times 10^{-7}$ can be excluded, for $m_{\rm in} \gtrsim 10^{7.2}$ g. In the bottom triangular region, which shows the parameter space where PBH generated ν_R do not rethermalize, the results correspond to the one discussed in Fig. 4. In this region, we have shown the $\Delta {\rm N}_{\rm eff}$ values for a particular value of $\beta = 10^{-8}$. In the right panel of Fig. 9, we show the constraint in the $m_{\rm in}$ versus β plane for a particular $G_{\rm eff}/G_{\rm F} = 10^{-6}$. Here, the region between the white dashed lines shows the parameter space leading to rethermalization. As expected from the left plot, here a stronger constraint on PBH mass can be seen.

V. GRAVITATIONAL WAVES FROM PBH DENSITY PERTURBATIONS

PBH can be involved in the generation of gravitational waves in several ways [59–61]. In this work, we focus on

[4]Considering a radiation-dominated universe during decoupling, the value of this critical decoupling temperature is found to be

$$T^{\rm crit}_{\rm dec} \simeq (T^2_{\rm ev} T_{\rm BH})^{1/3}. \tag{28}$$

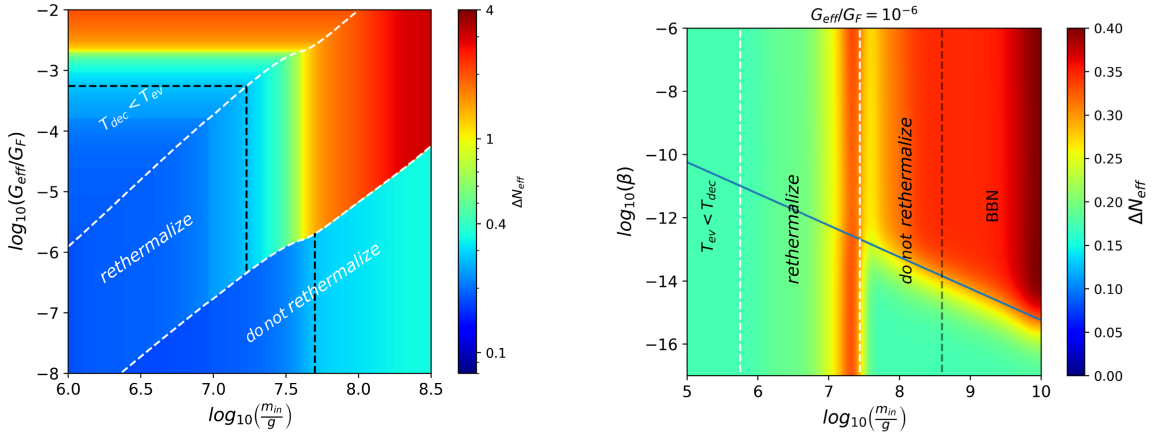

FIG. 9. Left: variation of ΔN_{eff} in m_{in}-G_{eff}/G_F plane for three different regions where (i) $T_{dec} < T_{ev}$, (ii) PBH generated ν_R rethermalize, and (iii) PBH generated ν_R do not rethermalize, separated by white dashed line. The dashed black colored line distinguishes the regions with $\Delta N_{eff} > 0.28$ and $\Delta N_{eff} < 0.28$. Right: variation of ΔN_{eff} in the m_{in}-β plane for a particular $G_{eff}/G_F = 10^{-6}$. A new constraint is obtained in the *rethermalized* region. The black vertical dashed line indicates the upper bound on PBH mass from BBN limit.

the gravitational waves induced by the density fluctuations of a PBH after their formation [62–64]. This is primarily because, for the PBH mass range we are working with, the GW spectrum produced through this route can be within the sensitivity of near-future GW experiments. Moreover, these induced gravitational waves are independent of the formation mechanism of PBH.

After the formation of PBHs, they are distributed randomly in space following Poissonian statistics [62]. These inhomogeneities in the distribution of PBHs induce curvature perturbations when the PBHs begin to dominate the energy density of the Universe, which at second order can source gravitational waves. The amplitude of these gravitational waves is further enhanced during the evaporation of the PBH. The dominant contribution to the present-day GW amplitude can be written as[5] [63,66,67]

$$\Omega_{gw}(t_0, f) \simeq \Omega_{gw}^{peak} \left(\frac{f}{f^{peak}}\right)^{11/3} \Theta(f^{peak} - f), \quad (29)$$

where Ω_{gw}^{peak} indicates the peak amplitude and is given by

$$\Omega_{gw}^{peak} \simeq 2 \times 10^{-6} \left(\frac{\beta}{10^{-8}}\right)^{16/3} \left(\frac{m_{in}}{10^7\ g}\right)^{34/9}. \quad (30)$$

Now, for length scales smaller than the mean separation between PBHs, the assumption of the PBH as a continuous fluid ceases to hold true. This imposes an ultraviolet cutoff to the GW spectrum, with f^{peak} corresponding to comoving scales representing the mean separation between PBHs. The peak frequency is found to be

$$f^{peak} \simeq 1.7 \times 10^3\ Hz \left(\frac{m_{in}}{10^4\ g}\right)^{-5/6}. \quad (31)$$

Since GWs behave like radiation, they can contribute to extrarelativistic degrees of freedom during BBN. This gives an upper bound on β, depending on PBH mass, which is given by [63]

$$\beta \lesssim 1.1 \times 10^{-6} \left(\frac{m_{in}}{10^4\ g}\right)^{-17/24}. \quad (32)$$

This upper bound on β for ultralight PBHs is stronger than other bounds, obtained, e.g., in Ref. [62] to avoid the backreaction problem.

Now, if PBHs play a role in sourcing the extrarelativistic degrees of freedom ΔN_{eff}, then the peak amplitude and the peak frequency of the GW spectrum discussed above would depend on the value of ΔN_{eff}, since m_{in} in Eqs. (30) and (31) is connected to ΔN_{eff}, as we have already seen in earlier discussions. Hence, observation of such a GW spectrum would provide a complementary probe to ΔN_{eff} observations at CMB experiments. In the left panel of Fig. 10, we show the GW spectrum arising from PBH density fluctuations, for different values of ΔN_{eff}, in the absence of extra interactions of the right-handed neutrinos. Note that such a GW spectrum is absent for the radiation-dominated case. For PBH domination, a higher value of ΔN_{eff} corresponds to a higher value of m_{in} (cf. Fig. 1), which shifts the peak frequency given by Eq. (31) to lower values. Any spectral line to the right of the one colored in dark cyan would correspond to the same value of $\Delta N_{eff} \simeq 0.16$, since PBH masses in that range evaporate above the electroweak scale, giving the same value of ΔN_{eff} (see Fig. 1). Here, β remains a free parameter since ΔN_{eff} is independent of β for PBH domination. In the right panel of

[5]The amplitude of the induced GW spectrum is sensitive to the PBH mass distribution [65]. Here, we consider a monochromatic mass spectrum for simplicity, as mentioned earlier.

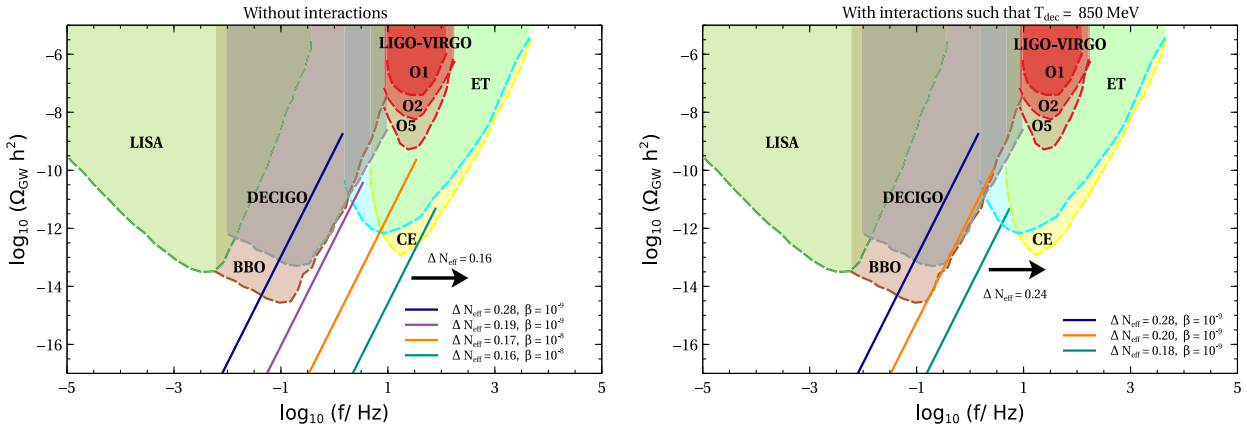

FIG. 10. GW spectra from PBH density fluctuations for different values of $\Delta N_{\rm eff}$, without extra interactions (left) and in the presence of extra interactions (right) of right-handed neutrinos. The various shaded regions indicate the future sensitivities and current bounds of GW detectors, which includes LISA, BBO, DECIGO, LIGO-VIRGO, ET, and CE. The arrows indicate a constant $\Delta N_{\rm eff}$ beyond a particular frequency (see text).

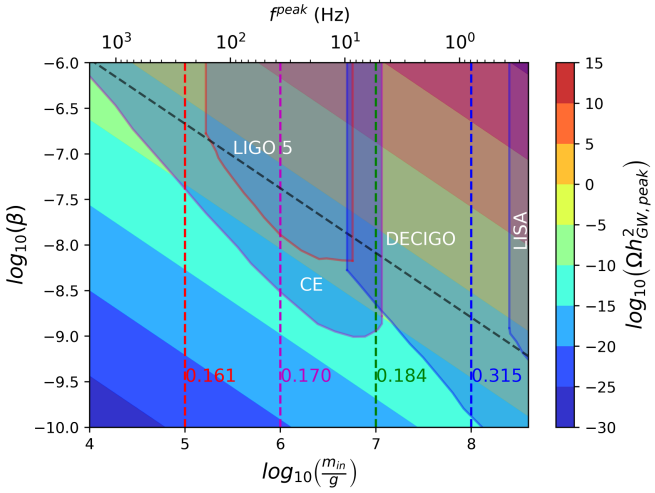

FIG. 11. Contours of peak amplitude of GWs induced by PBH density perturbations. The corresponding $\Delta N_{\rm eff}$ due to PBH generated ν_R are shown assuming no (or very feeble) ν_R-SM interactions. The black dashed line indicates the upper bound on β [cf. Eq. (32)].

Fig. 10, we show the GW spectra in the presence of extra interactions of right-handed neutrinos, with the strength of the interactions taken such that the thermal ν_R decouple at a temperature of ∼850 MeV. This case corresponds to the bottom right panel of Fig. 4. Here, any spectral line to the right of the one colored in dark cyan would correspond to the same value of $\Delta N_{\rm eff} = 0.24$, since PBHs in this mass range evaporate at a temperature higher than 850 MeV. Thus, the thermal contribution would dominate as discussed earlier, contributing to a total $\Delta N_{\rm eff}$ of 0.24, similar to the bottom right panel of Fig. 4. In both the plots shown in Fig. 10, the experimental sensitivities of relevant GW detectors, namely, LISA [68], DECIGO [69], BBO [70], ET [71], CE [72], and LIGO-VIRGO [73] are shown.

As we have seen already, the value of $\Delta N_{\rm eff}$ is independent of β for PBH domination. Thus, future observations of $N_{\rm eff}$ from CMB observations will not be able to tell us anything about β provided $\beta > \beta_{\rm crit}$. However, the value of β can be inferred from future GW detection with the spectral shape similar to the one generated by PBH density perturbations, since the peak of the GW amplitude is determined by β. In Fig. 11, we show the contours of the peak amplitude of GWs in the $m_{\rm in}$-β plane, indicating the values of $f_{\rm peak}$ and $\Delta N_{\rm eff}$, considering no extra interactions of ν_R with the SM. The future sensitivities of several GW experiments are also shown in the same figure. In the presence of extra interactions, the values of $\Delta N_{\rm eff}$ would be different as discussed above (cf. Fig. 10). $\Delta N_{\rm eff}$ values would also be different for other light species. Finally, we summarize the GW and CMB complementarities in Tables I and II by choosing a few

TABLE I. Without DR-SM interaction.

BP	$m_{\rm in}$ (g)	β	$\Delta N_{\rm eff}$			CMB experiment (2σ)			GW experiment
			ν_R	GB	MGB	ν_R	GB	MGB	
BP1	10^6	1.5×10^{-8}	0.167	0.052	0.023	CMB-S4	CMB-HD	None	CE, ET, LIGO-VIRGO
BP2	10^7	6×10^{-9}	0.183	0.056	0.024	CMB-S4	CMB-HD	None	CE, ET, DECIGO, BBO
BP3	10^8	6×10^{-10}	0.313	0.096	0.042	Planck	CMB-S4	CMB-HD	DECIGO, BBO

TABLE II. With DR-SM interaction.

				ΔN_{eff}			CMB experiment (2σ)			
BP	m_{in} (g)	β	T_{dec} (GeV)	ν_R	GB	MGB	ν_R	GB	MGB	GW experiment
BP1	10^6	1.5×10^{-8}	10	0.188	0.035	0.072	CMB-S4	CMB-HD	CMB-S4	CE, ET, LIGO-VIRGO
BP2	10^7	6×10^{-9}	0.8	0.242	0.046	0.092	CMB-S4	CMB-HD	CMB-S4	CE, ET, DECIGO, BBO
BP3	10^8	6×10^{-10}	0.01	3.02	0.575	1.15	Planck	Planck	Planck	DECIGO, BBO

benchmark points (BPs). PBH mass and initial energy fraction are fixed at benchmark values and the corresponding implications for ΔN_{eff} and GW observations for different types of dark radiation, namely, ν_R, Goldstone boson, and massless gauge boson are shown in Tables I and II. Note that we work with β values consistent with the upper bound given by Eq. (32) and higher than the critical value β_{crit} [cf. Eq. (7)] required for PBHs to dominate. While in Table I, no DR-SM interactions are assumed, in Table II, thermalized DR is considered with specific decoupling temperatures. While BP1 and BP2 in both cases remain within future sensitivities, BP3 for some specific type of DR is already ruled out by Planck 2σ limits.

VI. CONCLUSION

We revisit the prospects of generating dark radiation from primordial black holes in the early Universe, by considering sizable DR-SM interactions. We first reproduce the results by considering PBH and thermal interactions separately and the consequences for ΔN_{eff} observations at CMB experiments. We then consider the hybrid scenario with both thermal interactions and PBH to be the source of DR and put new constraints on the PBH parameters as well as DR-SM interactions from the requirement of satisfying BBN and CMB limits on ΔN_{eff}. Compared to the scenario with no DR-SM interactions discussed in earlier works, our present scenario puts tighter constraints on the PBH parameter space, namely, initial PBH mass and energy density.

We also find an interesting region of parameter space involving PBHs as well as DR-SM interactions where DR initially decouples from the bath followed by PBH evaporation, leading to rethermalization of DR with the SM bath. This leads to a lower decoupling temperature of DR enhancing the ΔN_{eff} and putting new constraints on the PBH parameter space. Though we have considered a specific type of DR, namely, light Dirac neutrinos for the numerical analysis, the generic conclusions are applicable to any thermalized DR.

We also find the gravitational wave complementarity of this scenario by considering PBH density perturbations to be the source of such stochastic GW. In the ultralight PBH window considered in our work, GWs sourced from PBHs this way not only remain within current and planned experiments' sensitivity, but also remains independent of PBH formation mechanisms. We show the complementarity between GW and CMB observations for different types of DR with and without DR-SM interactions. Interestingly, some of the benchmark points can lead to GW peak amplitude, frequency in the LIGO-VIRGO ballpark while keeping ΔN_{eff} within the reach of future CMB experiments like CMB-S4. On the contrary, some part of the parameter space can keep GW prospects within future experiments' reach while saturating Planck 2018 limits on ΔN_{eff}. Such complementary detection prospects at CMB and GW experiments of thermalized dark radiation are particularly interesting due to limited prospects of detecting such light degrees of freedom at particle physics experiments.

Before we end, we briefly comment on the impact of Kerr PBHs and a nonmonochromatic mass function of PBHs. First of all, considering a Kerr PBH does not significantly alter DR contribution to ΔN_{eff}. This is true for DR with spin 0, $1/2$, and 1, but significant enhancement is observed for spin 2 DR particles [26,74,75]. At the same time, our results on the analysis of the GW spectrum would almost be unchanged. This is mainly because the evaporation temperature of a spinning BH changes only slightly compared to the nonspinning case [76,77]. On the other hand, ΔN_{eff} can depend significantly on the mass distribution of a PBH. In Ref. [27], it was shown that the contribution to ΔN_{eff} might substantially change for some choices of the mass spectrum, compared to the monochromatic case. Similarly, the amplitude of induced GWs is also sensitive to the PBH mass spectrum [65,78]. It would be interesting to study the combined effect in the situation where DR is produced both from thermal bath (due to sizable DR-SM couplings) and from a PBH with nonmonochromatic mass distribution and nonzero spin distribution. We leave such a complete study for future works.

ACKNOWLEDGMENTS

N. D. would like to acknowledge Ministry of Education, Government of India for providing financial support for his research via the Prime Minister's Research Fellowship (PMRF) December 2021 scheme. S. J. D. thanks Dibyendu Nanda for some useful discussions related to this project. The work of D. B. is supported by the Science and Engineering Research Board (SERB), Government of India Grant No. MTR/2022/000575.

APPENDIX: NONSTANDARD INTERACTIONS OF DARK RADIATION

We consider the following effective operators for interactions among SM neutrinos and ν_R [46]:

$$\begin{aligned}-\mathcal{L} \supset\ & G_s\bar{\nu}_L\nu_R\bar{\nu}_L\nu_R + G_s^*\bar{\nu}_R\nu_L\bar{\nu}_R\nu_L + G_V\bar{\nu}_L\gamma^\mu\nu_L\bar{\nu}_R\gamma_\mu\nu_R \\ & + \tilde{G}_S\bar{\nu}_L\nu_R\bar{\nu}_R\nu_L + G_T\bar{\nu}_L\sigma^{\mu\nu}\nu_R\bar{\nu}_L\sigma_{\mu\nu}\nu_R \\ & + G_T^*\bar{\nu}_R\sigma^{\mu\nu}\nu_L\bar{\nu}_R\sigma_{\mu\nu}\nu_L, \end{aligned} \tag{A1}$$

where $G_S, \tilde{G}_S, G_V$, and G_T are effective coupling constants of respective four-fermion operators. The relevant processes that can lead to thermalization of ν_R are given by

$$\begin{aligned} &\nu_R + \nu_R \leftrightarrow \nu_R + \nu_R, \\ &\nu_R + \bar{\nu}_R \leftrightarrow \nu_L + \bar{\nu}_L, \\ &\nu_R + \nu_L \leftrightarrow \nu_R + \nu_L, \\ &\nu_R + \bar{\nu}_L \leftrightarrow \nu_R + \bar{\nu}_L, \\ &\nu_R + \bar{\nu}_L \leftrightarrow \bar{\nu}_R + \nu_L. \end{aligned} \tag{A2}$$

While we have focused on the case of right-handed neutrinos, interactions of other species of dark radiation with the standard model can also be realized through effective operators. For example, coupling of Goldstone bosons (ϕ) with the SM gauge sector at dimension 5 can be written as [79]

$$\mathcal{L} \supset -\frac{1}{4}\frac{\phi}{\Lambda}(c_1 B_{\mu\nu}\tilde{B}^{\mu\nu} + c_2 W_{\mu\nu}\tilde{W}^{\mu\nu} + c_3 G_{\mu\nu}\tilde{G}^{\mu\nu}), \tag{A3}$$

where $\{B_{\mu\nu}, W_{\mu\nu}, G_{\mu\nu}\}$ denotes the field strength tensor associated with SM gauge groups $\{U(1)_Y, SU(2)_L, SU(3)_c\}$, with $\{\tilde{B}^{\mu\nu}, \tilde{W}^{\mu\nu}, \tilde{G}^{\mu\nu}\}$ being their duals. Interaction of Goldstone bosons with the SM can also be realized through Yukawa couplings given by [79]

$$\mathcal{L} \supset -\frac{\partial_\mu\phi}{\Lambda_\psi}\bar{\psi}_1\gamma^\mu(g_V^{ij} + g_A^{ij}\gamma^5)\psi_j, \tag{A4}$$

where ψ denotes the SM fermions. Similar analysis performed in Sec. IV for Dirac neutrinos can be carried out to constrain the couplings of other species of dark radiation.

[1] Particle Data Group Collaboration, Review of particle physics, Prog. Theor. Exp. Phys. **2020**, 083C01 (2020).
[2] Planck Collaboration, Planck 2018 results. VI. Cosmological parameters, arXiv:1807.06209.
[3] L. Ackerman, M. R. Buckley, S. M. Carroll, and M. Kamionkowski, Dark matter and dark radiation, Phys. Rev. D **79**, 023519 (2009).
[4] D. N. Spergel and P. J. Steinhardt, Observational evidence for self-interacting cold dark matter, Phys. Rev. Lett. **84**, 3760 (2000).
[5] S. Tulin and H.-B. Yu, Dark matter self-interactions and small scale structure, Phys. Rep. **730**, 1 (2018).
[6] J. S. Bullock and M. Boylan-Kolchin, Small-scale challenges to the ΛCDM paradigm, Annu. Rev. Astron. Astrophys. **55**, 343 (2017).
[7] R. H. Cyburt, B. D. Fields, K. A. Olive, and T.-H. Yeh, Big bang nucleosynthesis: 2015, Rev. Mod. Phys. **88**, 015004 (2016).
[8] J. J. Bennett, G. Buldgen, P. F. De Salas, M. Drewes, S. Gariazzo, S. Pastor, and Y. Y. Y. Wong, Towards a precision calculation of $N_{\rm eff}$ in the Standard Model II: Neutrino decoupling in the presence of flavour oscillations and finite-temperature QED, J. Cosmol. Astropart. Phys. 04 (2021) 073.
[9] J. Froustey, C. Pitrou, and M. C. Volpe, Neutrino decoupling including flavour oscillations and primordial nucleosynthesis, J. Cosmol. Astropart. Phys. 12 (2020) 015.
[10] K. Akita and M. Yamaguchi, A precision calculation of relic neutrino decoupling, J. Cosmol. Astropart. Phys. 08 (2020) 012.
[11] G. Mangano, G. Miele, S. Pastor, T. Pinto, O. Pisanti, and P. D. Serpico, Relic neutrino decoupling including flavor oscillations, Nucl. Phys. **B729**, 221 (2005).
[12] E. Grohs, G. M. Fuller, C. T. Kishimoto, M. W. Paris, and A. Vlasenko, Neutrino energy transport in weak decoupling and big bang nucleosynthesis, Phys. Rev. D **93**, 083522 (2016).
[13] P. F. de Salas and S. Pastor, Relic neutrino decoupling with flavour oscillations revisited, J. Cosmol. Astropart. Phys. 07 (2016) 051.
[14] M. Escudero Abenza, Precision early Universe thermodynamics made simple: $N_{\rm eff}$ and neutrino decoupling in the Standard Model and beyond, J. Cosmol. Astropart. Phys. 05 (2020) 048.
[15] M. Cielo, M. Escudero, G. Mangano, and O. Pisanti, Neff in the standard model at NLO is 3.043, arXiv:2306.05460.
[16] K. Abazajian *et al.*, CMB-S4 science case, reference design, and project plan, arXiv:1907.04473.
[17] SPT-3G Collaboration, SPT-3G: A next-generation cosmic microwave background polarization experiment on the South Pole Telescope, Proc. SPIE Int. Soc. Opt. Eng. **9153**, 91531P (2014).
[18] Simons Observatory Collaboration, The Simons Observatory: Science goals and forecasts, J. Cosmol. Astropart. Phys. 02 (2019) 056.
[19] CMB-HD Collaboration, Snowmass2021 CMB-HD White Paper, arXiv:2203.05728.
[20] D. Hooper, G. Krnjaic, and S. D. McDermott, Dark radiation and superheavy dark matter from black hole domination, J. High Energy Phys. 08 (2019) 001.

[21] C. Lunardini and Y. F. Perez-Gonzalez, Dirac and Majorana neutrino signatures of primordial black holes, J. Cosmol. Astropart. Phys. 08 (2020) 014.
[22] M. J. Baker and A. Thamm, Black hole evaporation beyond the standard model of particle physics, J. High Energy Phys. 01 (2023) 063.
[23] M. J. Baker and A. Thamm, Probing the particle spectrum of nature with evaporating black holes, SciPost Phys. **12**, 150 (2022).
[24] F. Schiavone, D. Montanino, A. Mirizzi, and F. Capozzi, Axion-like particles from primordial black holes shining through the Universe, J. Cosmol. Astropart. Phys. 08 (2021) 063.
[25] A. Arbey, J. Auffinger, P. Sandick, B. Shams Es Haghi, and K. Sinha, Precision calculation of dark radiation from spinning primordial black holes and early matter-dominated eras, Phys. Rev. D **103**, 123549 (2021).
[26] A. Cheek, L. Heurtier, Y. F. Perez-Gonzalez, and J. Turner, Redshift effects in particle production from Kerr primordial black holes, Phys. Rev. D **106**, 103012 (2022).
[27] A. Cheek, L. Heurtier, Y. F. Perez-Gonzalez, and J. Turner, Evaporation of primordial black holes in the early Universe: Mass and spin distributions, Phys. Rev. D **108**, 015005 (2023).
[28] N. Bhaumik, A. Ghoshal, R. K. Jain, and M. Lewicki, Distinct signatures of spinning PBH domination and evaporation: Doubly peaked gravitational waves, dark relics and CMB complementarity, J. High Energy Phys. 05 (2023) 169.
[29] T. Fujita, M. Kawasaki, K. Harigaya, and R. Matsuda, Baryon asymmetry, dark matter, and density perturbation from primordial black holes, Phys. Rev. D **89**, 103501 (2014).
[30] B. Carr, K. Kohri, Y. Sendouda, and J. Yokoyama, Constraints on primordial black holes, Rep. Prog. Phys. **84**, 116902 (2021).
[31] I. Masina, Dark matter and dark radiation from evaporating primordial black holes, Eur. Phys. J. Plus **135**, 552 (2020).
[32] S. W. Hawking, Particle creation by black holes, Commun. Math. Phys. **43**, 199 (1975).
[33] S. Hawking, Gravitationally collapsed objects of very low mass, Mon. Not. R. Astron. Soc. **152**, 75 (1971).
[34] W. H. Press and P. Schechter, Formation of galaxies and clusters of galaxies by self-similar gravitational condensation, Astrophys. J. **187**, 425 (1974).
[35] M. Braglia, A. Linde, R. Kallosh, and F. Finelli, Hybrid α-attractors, primordial black holes and gravitational wave backgrounds, J. Cosmol. Astropart. Phys. 04 (2023) 033.
[36] K. Kawana and K.-P. Xie, Primordial black holes from a cosmic phase transition: The collapse of Fermi-balls, Phys. Lett. B **824**, 136791 (2022).
[37] T. Papanikolaou, Primordial black holes in loop quantum cosmology: The effect on the threshold, Classical Quantum Gravity **40**, 134001 (2023).
[38] J. H. MacGibbon, Quark and gluon jet emission from primordial black holes. 2. The lifetime emission, Phys. Rev. D **44**, 376 (1991).
[39] N. Bernal and O. Zapata, Dark matter in the time of primordial black holes, J. Cosmol. Astropart. Phys. 03 (2021) 015.
[40] Planck Collaboration, Planck 2018 results. X. Constraints on inflation, Astron. Astrophys. **641**, A10 (2020).
[41] Planck Collaboration, Planck 2018 results. VI. Cosmological parameters, Astron. Astrophys. **641**, A6 (2020).
[42] K. N. Abazajian and J. Heeck, Observing Dirac neutrinos in the cosmic microwave background, Phys. Rev. D **100**, 075027 (2019).
[43] P. Fileviez Pérez, C. Murgui, and A. D. Plascencia, Neutrino-dark matter connections in gauge theories, Phys. Rev. D **100**, 035041 (2019).
[44] D. Nanda and D. Borah, Connecting light Dirac neutrinos to a multi-component dark matter scenario in gauged $B-L$ model, Eur. Phys. J. C **80**, 557 (2020).
[45] C. Han, M. López-Ibáñez, B. Peng, and J. M. Yang, Dirac dark matter in $U(1)_{B-L}$ with Stueckelberg mechanism, Nucl. Phys. **B959**, 115154 (2020).
[46] X. Luo, W. Rodejohann, and X.-J. Xu, Dirac neutrinos and N_{eff}, J. Cosmol. Astropart. Phys. 06 (2020) 058.
[47] D. Borah, A. Dasgupta, C. Majumdar, and D. Nanda, Observing left-right symmetry in the cosmic microwave background, Phys. Rev. D **102**, 035025 (2020).
[48] P. Adshead, Y. Cui, A. J. Long, and M. Shamma, Unraveling the Dirac neutrino with cosmological and terrestrial detectors, Phys. Lett. B **823**, 136736 (2021).
[49] X. Luo, W. Rodejohann, and X.-J. Xu, Dirac neutrinos and N_{eff} II: The freeze-in case, J. Cosmol. Astropart. Phys. 03 (2021) 082.
[50] D. Mahanta and D. Borah, Low scale Dirac leptogenesis and dark matter with observable ΔN_{eff}, Eur. Phys. J. C **82**, 495 (2022).
[51] Y. Du and J.-H. Yu, Neutrino non-standard interactions meet precision measurements of N_{eff}, J. High Energy Phys. 05 (2021) 058.
[52] A. Biswas, D. Borah, and D. Nanda, Light Dirac neutrino portal dark matter with observable ΔNeff, J. Cosmol. Astropart. Phys. 10 (2021) 002.
[53] D. Borah, S. Mahapatra, D. Nanda, and N. Sahu, Type II Dirac seesaw with observable ΔN_{eff} in the light of W-mass anomaly, Phys. Lett. B **833**, 137297 (2022).
[54] S.-P. Li, X.-Q. Li, X.-S. Yan, and Y.-D. Yang, Effective neutrino number shift from keV-vacuum neutrinophilic 2HDM, Chin. Phys. C **47**, 043109 (2023).
[55] A. Biswas, D. K. Ghosh, and D. Nanda, Concealing Dirac neutrinos from cosmic microwave background, J. Cosmol. Astropart. Phys. 10 (2022) 006.
[56] A. Biswas, D. Borah, N. Das, and D. Nanda, Freeze-in dark matter via a light Dirac neutrino portal, Phys. Rev. D **107**, 015015 (2023).
[57] D. Borah, P. Das, and D. Nanda, Observable ΔN_{eff} in Dirac scotogenic model, arXiv:2211.13168.
[58] A. Cheek, L. Heurtier, Y. F. Perez-Gonzalez, and J. Turner, Primordial black hole evaporation and dark matter production: II. Interplay with the freeze-in/out mechanism, Phys. Rev. D **105**, 015023 (2022).
[59] R. Anantua, R. Easther, and J. T. Giblin, GUT-scale primordial black holes: Consequences and constraints, Phys. Rev. Lett. **103**, 111303 (2009).
[60] J. L. Zagorac, R. Easther, and N. Padmanabhan, GUT-scale primordial black holes: Mergers and gravitational waves, J. Cosmol. Astropart. Phys. 06 (2019) 052.
[61] R. Saito and J. Yokoyama, Gravitational wave background as a probe of the primordial black hole abundance, Phys. Rev. Lett. **102**, 161101 (2009).

[62] T. Papanikolaou, V. Vennin, and D. Langlois, Gravitational waves from a universe filled with primordial black holes, J. Cosmol. Astropart. Phys. 03 (2021) 053.
[63] G. Domènech, C. Lin, and M. Sasaki, Gravitational wave constraints on the primordial black hole dominated early Universe, J. Cosmol. Astropart. Phys. 04 (2021) 062.
[64] G. Domènech, V. Takhistov, and M. Sasaki, Exploring evaporating primordial black holes with gravitational waves, Phys. Lett. B **823**, 136722 (2021).
[65] T. Papanikolaou, Gravitational waves induced from primordial black hole fluctuations: The effect of an extended mass function, J. Cosmol. Astropart. Phys. 10 (2022) 089.
[66] D. Borah, S. Jyoti Das, R. Samanta, and F. R. Urban, PBH-infused seesaw origin of matter and unique gravitational waves, J. High Energy Phys. 03 (2023) 127.
[67] B. Barman, D. Borah, S. Jyoti Das, and R. Roshan, Gravitational wave signatures of a PBH-generated baryon-dark matter coincidence, Phys. Rev. D **107**, 095002 (2023).
[68] LISA Collaboration, Laser interferometer space antenna, arXiv:1702.00786.
[69] S. Kawamura *et al.*, The Japanese space gravitational wave antenna DECIGO, Classical Quantum Gravity **23**, S125 (2006).
[70] K. Yagi and N. Seto, Detector configuration of DECIGO/BBO and identification of cosmological neutron-star binaries, Phys. Rev. D **83**, 044011 (2011).
[71] ET Collaboration, The Einstein Telescope: A third-generation gravitational wave observatory, Classical Quantum Gravity **27**, 194002 (2010).
[72] LIGO Scientific Collaboration, Exploring the sensitivity of next generation gravitational wave detectors, Classical Quantum Gravity **34**, 044001 (2017).
[73] LIGO Scientific Collaboration, Advanced LIGO, Classical Quantum Gravity **32**, 074001 (2015).
[74] D. Hooper, G. Krnjaic, J. March-Russell, S. D. McDermott, and R. Petrossian-Byrne, Hot gravitons and gravitational waves from Kerr black holes in the early Universe, arXiv:2004.00618.
[75] I. Masina, Dark matter and dark radiation from evaporating Kerr primordial black holes, Gravitation Cosmol. **27**, 315 (2021).
[76] R. Dong, W. H. Kinney, and D. Stojkovic, Gravitational wave production by Hawking radiation from rotating primordial black holes, J. Cosmol. Astropart. Phys. 10 (2016) 034.
[77] A. Arbey, J. Auffinger, and J. Silk, Evolution of primordial black hole spin due to Hawking radiation, Mon. Not. R. Astron. Soc. **494**, 1257 (2020).
[78] G. Domènech, Scalar induced gravitational waves review, Universe **7**, 398 (2021).
[79] D. Baumann, D. Green, and B. Wallisch, New target for cosmic axion searches, Phys. Rev. Lett. **117**, 171301 (2016).